Gyres Driven by Combined Wind and Buoyancy Flux*

JAMES LUYTEN AND HENRY STOMMEL

Woods Hole Oceanographic Institution, Woods Hole, MA 02543

(Manuscript received 6 August 1985, in final form 3 February 1986)

ABSTRACT

The combined effects of buoyancy forcing and wind in a gyre-scale steady ocean circulation are modeled using discrete layers with an interfacial flux, not necessarily vertical. The equations for vorticity conservation of the geostrophic flow in this system are fully nonlinear, involving a Jacobian for the layer thicknesses. These equations are written in a form which can be solved by the method of characteristics. The form of these equations invites the interpretation that the geostrophic baroclinic flow is driven by buoyancy and steered by the wind. Two examples are solved and discussed, a subtropical gyre with heating, and a subpolar gyre with cooling. In each case, there are distinct regimes of flow, depending upon whether the characteristics originate at the eastern or western boundaries of the model. A simple geometrical argument illustrates that the difference between these two regimes, the direct and indirect cells, depends upon the sign of the true vertical velocity relative to the interfacial flux.

1. Introduction

Ever since the controversy between Carpenter and Croll over a century ago, we have been somewhat unclear about the relative roles of wind stress and buoyancy flux in driving the ocean circulation. Wind stress has led the field ever since Ekman's theory of the frictional spiral. In the formulations of Sverdrup, Stommel and others, wind stress was chosen because of its simplicity, and various simple models worked out. A parallel set of simple models involving buoyancy flux was not developed, and as a result a generation of textbook writers has elevated this one-sidedness to a dogma.

The main difficulty of incorporating buoyancy flux divergence into layered models lies in the nonlinearity of the Jacobians of interface depths that appear in the vorticity equations. Such terms are of course incorporated in large numerical models but their physical role has remained obscure because of the numerical fog. The purpose of this paper is to present the solution of two examples subject to both wind stress and buoyancy flux, containing an active Jacobian of interface depths, but so simple that much of the behavior can be qualitatively inferred directly from characteristic equations—and the use of a small personal computer reserved for working out the quantitative details. In this way we think we are able to show something of how the combined driving agents call up different roles for the Jacobian in different geographical regions. For example, one might ask: "Do the wind stress and buoyancy flux together produce solutions that are the sum of those produced when they act separately?" We will show that in some parts of the ocean they do, and in other regions they do not.

In setting up the models, we have kept the North Atlantic Ocean in mind. Indeed this study is an outgrowth of the diagnostic study of the northern North Atlantic by Luyten et al. (1985), the note on beta-wave controls in layered zonal flows acted upon by buoyancy flux by Luyten and Stommel (1985b) and the earlier theory of the purely wind-driven ventilated thermocline by Luyten et al. (1983).

The two examples that we present here are: Case A, a complete subtropical gyre driven by downward Ekman pumping and a buoyancy flux that changes sign at some midlatitude within the gyre. Case B, the equatorward half of the subpolar gyre driven by upward Ekman suction and buoyancy loss. We will treat these two cases separately, reserving a discussion of the interaction between gyres for a future communication.

2. The characteristic equation

Let h, D be the depths of two interfaces bounding three layers of differing density, the deepest of which is a rest, as shown in Fig. 1. The equations for volume conservation in the two moving uppermost layers are

$$[hu_1]_x + [hv_1]_y = w_s - w_e$$

$$[(D-h)u_2]_x + [(D-h)v_2]_y = -w_s$$

where $u_{1,2}$ and $v_{1,2}$ are the horizontal components of velocity in the top and lower layer, the upward (vertical) Ekman suction is w_e and the interfacial flux into the upper layer across the upper interface is w_s, not nec-

* Contribution Number 6017 of the Woods Hole Oceanographic Institution.

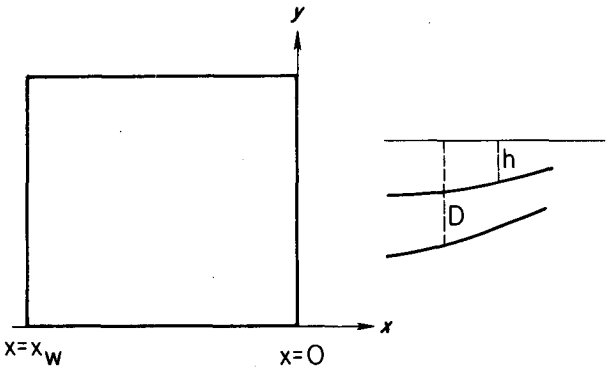

FIG. 1. Geometry of the two layer model.

essarily vertical. The quantity g' is the reduced gravity across each interface, and the Coriolis parameter is $f = \beta y$. We will generally be working some distance from the equator. Taking the velocities to be steady and geostrophic in the interior of the ocean

$$u_2 = -\frac{g'}{f} D_y, \quad v_2 = \frac{g'}{f} D_x$$

$$u_1 = -\frac{g'}{f} (h_y + D_y), \quad v_1 = \frac{g'}{f} (h_x + D_x)$$

and introducing them into the first two layer equations we obtain

$$\frac{g'}{f} [-h_x(D_y + h_y) + h_y(D_x + h_x)] - \frac{\beta g'}{f^2} h(D_x + h_x) = w_s - w_e \quad (1a)$$

$$\frac{g'}{f} [-(D - h)_x D_y + (D - h)_y D_x] - \frac{\beta g'}{f^2} (D - h) D_x = -w_s \quad (1b)$$

or

$$\frac{g'}{f} [-h_x D_y + h_y D_x] - \frac{\beta g'}{f^2} h(D_x + h_x) = w_s - w_e \quad (2a)$$

$$-\frac{g'}{f} [-h_x D_y + h_y D_x] - \frac{\beta g'}{f^2} (D - h) D_x = -w_s. \quad (2b)$$

Strictly speaking, the entire left-hand side of these equations is each a single Jacobian, but the "twisting terms" are here isolated in the first term, and separated from the familiar beta term. It is the twisting terms that we are particularly anxious not to avoid, because we want to explore their physical role.

We proceed by summing the two equations and then integrating to get the familiar relations:

$$\frac{\beta g'}{f^2} (hh_x + DD_x) = w_e$$

$$\frac{1}{2} [h^2 + D^2] = \frac{1}{2} (h_0^2 + D_0^2) + \int_{x_0}^{x} \frac{f^2 w_e}{\beta g'} dx'. \quad (3a)$$

For simplicity, at this point, we take w_e to be independent of x and $x_0 = 0$ so that we have

$$\frac{1}{2} (h^2 + D^2) = \frac{1}{2} (h_0^2 + D_0^2) + W_e x \quad (3b)$$

where $W_e = f^2 w_e / \beta g'$ and h_0, D_0 are the values of h and D at $x_0 = 0$.

We then differentiate with respect to y to get

$$\left.\begin{aligned} hh_y + DD_y &= W_{ey} x \\ hh_x + DD_x &= W_e \end{aligned}\right\}$$

and then substitute these into Eq. (2b) to eliminate the derivatives h_x and h_y:

$$-\frac{g'}{f}\left[-\left(-D\frac{D_x}{h} + \frac{W_e}{h}\right) D_y + -D\frac{D_y}{h} + \frac{W_{ey}}{h} \cdot x D_x\right] - \frac{\beta g'}{f^2} (D - h) D_x = -w_s.$$

Multiplying by h/D and simplifying, we find

$$\left(g' \frac{W_e}{fD}\right) D_y + \left[-\frac{g' x W_{ey}}{fD} - \frac{\beta g' h(D - h)}{f^2 D}\right] D_x = -h \frac{w_s}{D}.$$

An equation similar to this was obtained by Veronis (1978) who suggested that it could be solved iteratively to provide a correction to the linear solution. No such restriction, however, is required. This equation is, unexpectedly, a first-order linear partial differential equation in D only, with what at first sight seems to be somewhat complicated and unpleasant coefficients, but it can be integrated along characteristics. Although the variable h appears explicitly in this equation it can always be evaluated using the Sverdrup equation (3b). So, in essence, this is an equation for determining the depth of the lower interface, D, starting at certain specified boundary values, and knowing the two driving agents w_s and w_e.

The characteristic velocities u_c and v_c are

$$\frac{dx}{ds} = u_c = -\frac{g'}{f} \frac{W_{ey} \cdot x}{D} - \frac{\beta g'}{f^2} \frac{h(D - h)}{D} \quad (4a)$$

$$\frac{dy}{ds} = v_c = \frac{g'}{f} \frac{W_e}{D} \quad (4b)$$

and the rate of change of D at a point moving along the characteristic (with increasing arc length s) is

$$\frac{dD}{ds} = -\left(\frac{h}{D}\right) w_s. \quad (4c)$$

The characteristic velocities are of course not the same as the particle velocities of the fluids. What are they, then, from a physical point of view? The northward component of the characteristic velocity can be written in the form

$$v_c = \frac{g' W_e}{fD} = \frac{g'}{fD} (hh_x + DD_x) = \frac{1}{D} [hv_1 + (D - h)v_2],$$

which is the northward Sverdrup velocity averaged over the two top layers. The eastward component of the characteristic velocity is the sum of two terms

$$u_c = -\frac{g'x \cdot W_{ey}}{fD} - \frac{\beta g' h(D-h)}{f^2 D}$$

$$= \frac{hu_1 + (D-h)u_2}{D} - \frac{\beta g' h(D-h)}{f^2 D}.$$

The first term is the vertically averaged (over the top two layers) zonal Sverdrup transport; the second term is the westward nondispersive internal Rossby-wave propagation velocity. It is the possibility of balance of the two terms in the eastward characteristic velocity that leads to the critical conditions in Luyten and Stommel (1985b).

It is tempting to describe the relative role of the two driving agents in a language that follows from the form of the characteristic equation itself. Noting that the Ekman suction $\bar{W}_e$ and its derivative $\bar{W}_{ey}$ appear explicitly in the characteristic velocities, and hence determine their speed and direction, whereas the interfacial flux $\bar{w}_s$ appears on the right-hand side as the term which explicitly changes the depth of D (and h), we might risk saying: "The baroclinic ocean circulation is driven by buoyancy and is steered by wind." It may also be worth mentioning that the patterns of flow that emerge are much more complicated than those envisaged in the old linear theory of the abyssal circulation given by Stommel (1957).

3. Case A: Model of the subtropical gyre

For a model of the subtropical gyre we use a formulation similar to the ventilated thermocline (Luyten et al., 1983). We choose the (scaled) Ekman pumping W_e as a negative half sine wave, so that the total Sverdrup transport vanishes at the northern and southern boundaries (Fig. 2). We assume that the upper layer outcrops ($h = 0$) along the central latitude circle. We assume that there is no geostrophic flow across the eastern boundary, at $x = 0$, so that $D = D_0$ and $h = 0$. Our choice of the form of the buoyancy flux W_s is shown in the figure corresponding to cooling north of a latitude y_i where W_s passes through zero, and heating south of that latitude. The form of the characteristic equations (4) insured that the effects of the buoyancy flux vanish when h vanishes; therefore we set $W_s = 0$ when $h = 0$. There is another important latitude y_s at which $W_s = W_e$, which we encounter again later.

For our particular choice of W_s, vanishing along the southern boundary, D and h are constant along that southern boundary and therefore no mass flux across that latitude. We make this choice in order to isolate the effects of the buoyancy flux within the gyre, uncomplicated by cross-gyre mass fluxes arising from nonzero W_s along the gyre boundaries.

For more general distributions of buoyancy flux, mass fluxes can occur across both the northern and southern boundaries, but inasmuch as the characteristic velocity v_c vanishes at both the northern and southern boundaries ($W_e = 0$) characteristics can never originate there, but move southward ($W_e < 0$) in between.

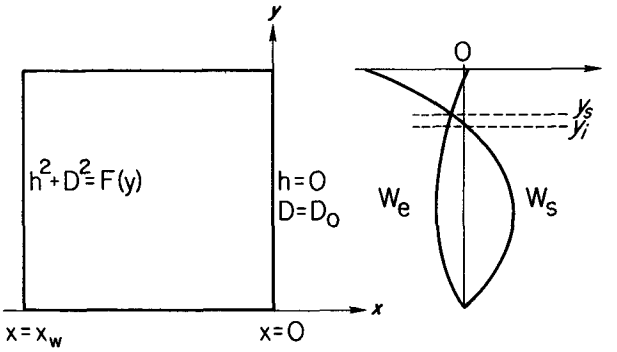

FIG. 2. Geometry of the subtropical gyre model. The meridional dependence of the functions representing the interfacial flux (W_s) and the Ekman suction (W_e) are shown on the right. Note that the factor $f^2/\beta g'$ is included. It is assumed that $h = 0$ in the northern half of the gyre.

Therefore characteristics must come into the model space from the east and/or the west. Along the western wall the eastward component u_c of the characteristic velocity indicates that they cannot enter from the southern half of the western boundary, where $W_{ey} > 0$, even if water in one layer does. It is only in the northern half of the western wall where $W_{ey} < 0$ and $h = 0$ that characteristics can enter.

There is a degree of arbitrariness about the boundary conditions along the western wall. If we expect a continuous solution for the layer depths, the values $h(x_w, y)$ and $D(x_w, y)$ must conform to the Sverdrup relation, Eq. (3b). Otherwise, they can be chosen arbitrarily, to represent the inflow from the western boundary current. In the solutions discussed here we have chosen, for simplicity, only inflow in the lower layer in the northern half of the gyre where the characteristics enter from the western boundary. Other assumptions could be made which change the quantitative behavior of the solutions; some of these are discussed by Luyten et al. (1983).

On the eastern wall (Fig. 3) $h = 0$, so both terms of u_c vanish and it might seem that characteristics cannot enter there. In latitudes where $h > 0$ away from the eastern wall, and infinitesimally close to the wall where $D = D_0$ and $h = 0$, we assume $h_y = D_y = 0$ and have

$$\left.\begin{aligned} h(D_x + h_x) &= W_e - W_s \\ (D-h)D_x &= W_s \end{aligned}\right\}$$

which can be combined to give ($h \ll D$)

$$\frac{\partial}{\partial x}\left(\frac{h^2}{2}\right) = W_e - W_s, \quad \frac{\partial}{\partial x}\left(\frac{D^2}{2}\right) = W_s. \qquad (5)$$

Thus, we evaluate h and D at the first grid point ($\delta x < 0$) in from the eastern wall as

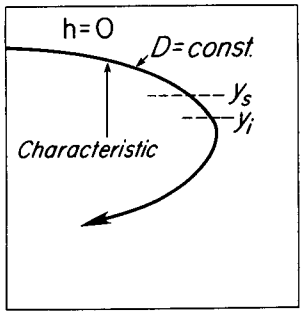

FIG. 3. Detailed geometry of the characteristic calculation and at the subduction latitude.

$$h^2\,(x = \delta x,\, y) = 2(W_e - W_s)\delta x \tag{6}$$

$$D^2\,(x = \delta x,\, y) = D_0{}^2 - 2W_s\delta x. \tag{7}$$

These values of $h(\delta x, y)$, $D(\delta x, y)$ are then used as initial conditions for the characteristic calculation where now $u_c < 0$ and the characteristic can proceed on its way accumulating changes in D and h as it moves southwestward. Note that since $\delta x < 0$ and $W_e < 0$, h will not increase unless $W_s > W_e$, otherwise the upper layer water pumped by the Ekman convergence will be cooled ($W_s \leqslant W_e < 0$) and pass into the deeper layer directly.

A similar hurdle presents itself to characteristics entering the model space from the northern half of the western wall. Those that begin with $h = 0$ first follow characteristics governed entirely by u_c that has no second term, and along which D does not change (Fig. 3b). In this portion of the space where $h = 0$ the characteristic follows the geostrophic contours of the lower exposed layer and columns of this water move along it. The Ekman pumping from above is adding water to the top of the moving water column; that is indeed necessary to allow for the necessary shrinkage of the rest of the column as it approaches lower latitude.

Eventually this characteristic encounters the latitude y_s where $W_s = W_e$. At this point more water from the Ekman layer can accumulate than is lost by buoyancy flux to the lower layer, so here it is possible for the upper layer to begin to form, and we can have an $h > 0$. The lower layer subducts where the upper layer forms.

In order to allow the calculation along the characteristic to pass through the latitude of subduction y_s, it is necessary to use a special procedure for the first step of integration as before. Taking Eq. (1) with $h = 0$

$$\frac{g'}{f}\,[-h_x D_y + h_y D_x] = W_s - W_e$$

and Eq. (3) also with $h = 0$

$$DD_x = W_e; \quad DD_y = W_{ey}x$$

and substituting, we obtain

$$\frac{g'}{f}\,[-W_{ey}xh_x + W_e h_y] = D(W_s - W_e). \tag{8}$$

Inasmuch as W_s and W_e are functions of y only, we anticipate that, near $h = 0$, $h_x = 0$, and hence we can use the following equation as our starting step, to carry the characteristic through subduction,

$$h_y = \frac{\beta}{f} D(W_s - W_e)/W_e. \tag{9}$$

This result can be generalized easily for a curved subduction line $y_s(x)$.

To get a proper slope at subduction ($h_y < 0$) in a region with $W_e < 0$, we must have $W_s - W_e > 0$, which occurs south of y_s. The slope can start with a nonzero value if we imagine that the warm water comes from the Ekman layer directly by the pumping down, and that it is delayed to some latitude south of the latitude y_s as defined above. Then subduction will begin with a finite slope, given by Eq. (9) where the right-hand side is already finite. This is probably a way to think of the problem consistent with the earlier model of the ventilated thermocline (Luyten et al., 1983).

A sample run of Case A is exhibited in Fig. 4, with the amplitude of $w_e = -3$ cm day^{-1}, $w_s = 3$ cm day^{-1} and $D_0 = 150$ meters. The parameters for this sample case are appropriate for the upper thermocline in the subtropical gyre. It is not our purpose here to develop a complete model of the subtropical gyre; we leave that to future communications.

The characteristics and their regimes are shown in Figs. 4a and 4b. The boundary between the regimes is marked as the curve B. The eastern regime corresponds to the "shadow zone" of the ventilated thermocline model, but here it is ventilated by interfacial flux. The Rossby control point R_c where both components of the characteristic velocity vanish is located in the northeastern corner of the gyre. The north–south symmetrical Sverdrup transport function $h^2 + D^2 - D_0{}^2$ (insensible to W_s) is shown in Fig. 4c. The depth h of the upper interface is shown in Fig. 4d. The maximum depth of h is south of the maximum of the Sverdrup transport.

The depth D of the lower interface (Fig. 4f) parallels the Sverdrup transport function in the region north of y_s. After subduction the contours of D still are the contours of geostrophic flow in the lower layer, so arrows are attached to them to indicate the direction of flow. There is a cyclonic gyre that occupies the "shadow zone" of the old ventilated thermocline theory of Luyten et al. (1983). At latitudes along the common edge of the two opposing gyres in the lower layer there is a strong westward flow that may have some connection with the spread of Mediterranean Water in the North Atlantic.

The flow in the upper layer is governed by the pressure field $h + D$ and is shown in Fig. 4e. Arrows are attached to the contours to indicate directions of flow. There is only one gyre, displaced to the southward of that shown in the Sverdrup transport. South of y_s the flow is directed from shallow to deep upper layer as

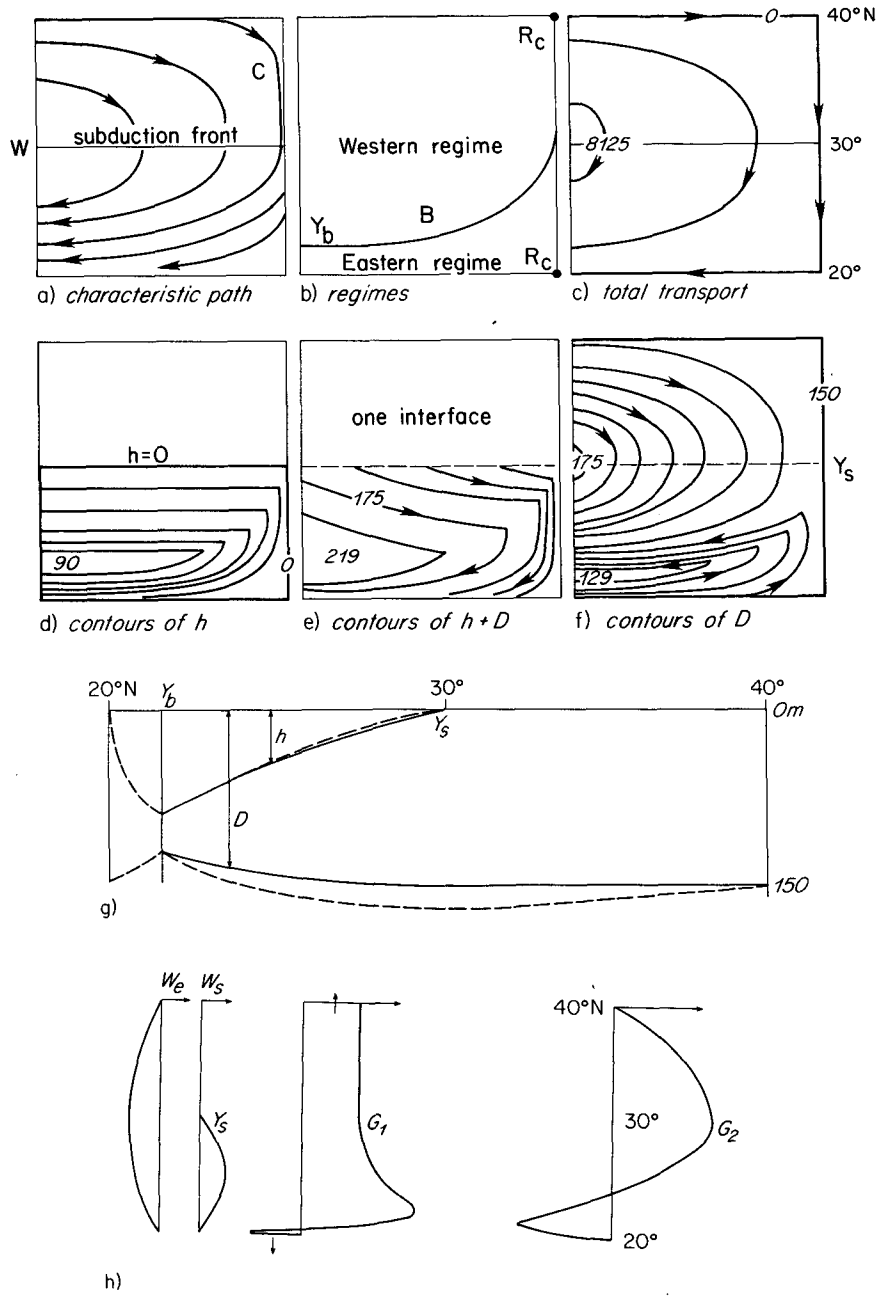

FIG. 4. Case A (the subtropical gyre): parameters w_e = 3 cm day^{-1}; w_s = −3 cm day^{-1}; x_w = −2000 km; midlatitude = 30°N; h_0 = 0 m; D_0 = 150 m; g' = 0.01 m s^{-2}. The panels show (a) paths of characteristics, (b) regimes and curve of u_e = 0, (c) Sverdrup transport function $h^2 + D^2$ (m^2) with contours of 5 m^2 and (d), (e), (f) the quantities h, $h + D$ and D with contours of 15, 5 and 4 m, respectively. Panel (g) shows a vertical section along the separating characteristic C (solid) and along the western wall (w) projected along a meridian. Panel (h) shows the wind and buoyancy forcing, upper and lower layer transports in the western boundary region.

must be the case where there is a nonvertical positive w_s.

One of the interesting features of the velocity field indicated in Figs. 4e and 4f is the eastern intensification of the meridional components of velocity in both layers, associated with the counterclockwise twist of the centers of the two lower-layer gyres that comes from the form of the boundary characteristic B.

For characteristics in the eastern regime, the flow in the upper layer is nearly parallel but opposite to the deep flow. The vertical component of velocity w_1 at the interface as computed from the vorticity equation

$\beta v = f(\partial w/\partial z)$ has the same sign as w_s (>0). Luyten and Stommel (1985b) have termed this a direct cell.

For characteristics in the western regime, there is a strong velocity spiral between the upper and lower layers with the twisting terms playing a crucial role in the dynamics. In this region the vertical component of velocity at the interface is actually negative, and it is the spiral that allows this to be consistent with the upward forcing imposed by the positive w_s.

In the western regime, however, the cell is indirect, because the w_1 is actually negative, and points downward, and it is the spiral that allows this to be consistent with the upward forcing imposed by a positive w_s.

Figure 4g shows two vertical sections projected on the meridional plane. The solid one shows both h and D along the characteristic C, the lower half of which coincides with the boundary B as functions of latitude. In the northern portion there is just a single layer because we have imposed $h = 0$ at the beginning of these characteristics along the western boundary. We could have done otherwise; it is just somewhat complicated, and the upper layer could be shown to become shallower, and even vanish, if sufficiently cooled there. At y_s the upper layer begins to form, initially, in this simple case with a slope $h_y(y_s) = -\beta D/f$ [Eq. (9), $w_s = 0$]. Because the slope of h in this case is stronger than that of D below, there is an eastward component of flow of upper layer water across the boundary B, despite the westward component of flow across B in the lower layer. This latter flow is entirely supplied by the low-latitude cyclonic gyre in the lower layer, induced by w_s in the eastern regime where otherwise there would be a "shadow zone". This section stops at the intersection of B with the western wall, y_b. The other section shown in dashed line format is that along the western wall. The northern half of this is computed from the Sverdrup relation assuming that there is no upper layer. Its depth increases as latitude decreases, as expected. (Note this is not the case along characteristic C in this range of latitude). This slope reverses at the latitude of maximum Sverdrup transport, which in this case is also y_s. The depth D reaches a minimum at y_b and then increases to its prescribed wall value at the southern wall. The upper layer h nearly parallels its counterpart along C between y_s and y_b and then rapidly thins out to zero at the southern wall. Between latitudes y_b and 20°N we have the direct cell of the cyclonic gyre in the eastern regime along the western wall.

The transports across the western wall feed a western boundary current. In Fig. 4h we have sketched one possible interpretation of the meridional boundary current transports for each layer, as functions of latitude for the upper layer G_1 and lower layer G_2.

The lower layer is easiest to understand. It receives, in this example, water from the Ekman layer in the northern half of the subtropical gyre, and loses an equivalent amount to the upper layer in the southern half by the flux w_s. Therefore we can begin the integration of the equation for the G_2 function

$$G_2(y) = \int_{20°}^{y} u_2(D - h)dy \tag{10}$$

from zero at the lower latitude limit and it will return to zero at the upper limit, as shown. The northern half of this transport is simply the one-layer Sverdrup transport associated with the Ekman driving. The sharp reversal in the lower half reflects the influence of the cyclonic gyre that bestrides the boundary B.

In trying to set the zero of the G_1 function, however, it is necessary to recall that the gyre receives water from an Ekman flux over its whole surface, roughly half from the north and half from the south. The transport at the lower latitude limit can be set to compensate for these inflows, as shown, so that half goes south at the southern limit, and half north at the northern limit. Because we have assumed that there is no upper layer water flowing into the gyre along the western wall in the northern half of the gyre, we must allow G_1 to remain constant there. The interpretation of this state of affairs is that the water carried southward out of the system in the upper layer is eventually returned to the gyre through the Ekman flux, but since it is already hot it does not need to be heated. There is no heat flux across the southern boundary therefore. On the other hand, the upper layer that escapes to the north of the gyre in the boundary current has to be cooled to return to cool water Ekman supply in the northern half of the gyre. It therefore represents the needed northward heat transport out of the gyre, which of course is necessary to balance the whole system.

It is necessary to emphasize that the decision to exclude upper layer water from entering the northern half of the gyre across the western wall is entirely arbitrary. We have experimented with other choices, and all that they do is to introduce Rhines-Young (1982) regions. To remove this degree of freedom we need some restrictions of a dynamical nature within the western boundary current itself, presumably of the kind outlined by Luyten and Stommel (1985a) in a study of two layer inertial Gulf Streams, but this presents technical difficulties beyond the scope of this paper to which we have not addressed ourselves.

4. Case B: Model of the subpolar gyre

The geometry of our model of the equatorward half of the subpolar gyre is shown in Fig. 5. In order to assure no geostrophic flow through the eastern wall we take h and D to have the constant values h_0 and D_0 at this longitude $x = 0$. Instead of assuming that h_0 vanishes at the eastern wall $x = 0$, we give it a finite value. This means that there is a finite Rossby wave velocity at the wall, and since there is no Sverdrup zonal velocity at the wall, characteristics move freely westward from all points of the wall. As we will see, this can lead to points of vanishing characteristic velocity within the interior, which repel all characteristics that approach them. We will call such points "Rossby repellors." The

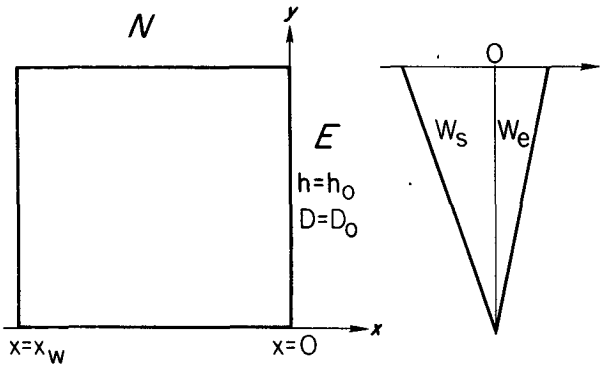

FIG. 5. Geometry of the subpolar model. The meridional dependence of the functions representing the interfacial flux (W_s) and the Ekman suction (W_e) are shown on the right. Note that the factor f^*f/bg' is included.

forcing functions W_e and W_s are assumed to be simple linear ramps, increasing from zero at the southern latitude $y = y_s$ to a maximum at the northern boundary latitude. Considering now the characteristic velocities, we notice that the northward component v_c is positive everywhere except that it vanishes at the southern boundary, so no characteristics can emerge northward from there. As already noted, the eastward component of the characteristic velocity u_c is negative right on the eastern wall, $x = 0$, so characteristics do emerge from this wall toward the northwest. The eastward Sverdrup transport increases toward the west, so that these characteristics encounter an eastward directed zonal Sverdrup flow as they move westward, and hence move more directly northward. Far to the west on the western boundary itself, at $x = x_w$ where $x_w \ll 0$, the positive first term in u_c overpowers the Rossby-wave term. Thus, characteristics may also be expected to enter the region of the model from the western boundary as well. The choice of h and D along the western boundary is constrained (if the solution within the box be continuous) by the Sverdrup relation [Eq. (3b)] but there is still one degree of freedom which can be chosen arbitrarily. Whether this degree of freedom on the western boundary is ultimately controlled upstream by a Bernoulli control in the western boundary current that feeds it, or by other requirements imposed by joining to the subtropical gyre, we must defer for the present. In this regard one should remember that we are also treating h_0 and D_0 as given, whereas in a physical system they might be expected to find their own values. As characteristics move in from the western wall they turn northward, their eastward velocity diminishes, and they may even enter a region where the westward directed Rossby-wave term predominates and turns them back westward again at a higher latitude. Because of the extra degree of freedom on the western boundary we have to make an arbitrary decision there. We choose for illustration's sake $D = D_0$ on $x = x_w$ and compute from both western and eastern boundaries using the characteristic equation (4).

Figure 6a shows the paths and directions of the characteristics entering from both sides. They all have a northward trend that increases in speed with latitude and with W_e. In Fig. 6b we show the different regimes and the boundary B between them. This boundary originates at the Rossby-wave control point R_c which is the only point in the space of the model where both characteristic velocity components vanish simultaneously. It acts as a repeller to the characteristics. The dashed curves are the loci of vanishing u_c in the rest of the gyre—they are distinct from the regime boundary B. The eastern regime "knows" about the values of both h and D on the eastern boundary but the western regime only knows them through the integrated Sverdrup condition at $x = x_w$. The total Sverdrup transport is illustrated in Fig. 6c; it doesn't know about the characteristics nor does it give any indication of the existence of the regimes in Figs. 6a and 6b. The Sverdrup transport function is the sum of the transports in the two moving layers, and they are, individually, as can be seen from Figs. 6d–f, sensitive to the location of the regimes. The general trends of the layer depths h and D and of the pressure $h + D$ in the upper layer are qualitatively evident from the form of their characteristic equations,

$$\frac{dh}{ds} = -W_e\left(1 - \frac{h}{D}\right) + W_s \qquad (11a)$$

$$\frac{dD}{ds} = -W_s\frac{h}{D} \qquad (11b)$$

$$\frac{d(h+D)}{ds} = (W_s - W_e)\left(1 - \frac{h}{D}\right) \qquad (11c)$$

where we have used the scaled form of w_s introduced earlier. In Case B, since $h > 0$, $D > 0$, $D - h > 0$, $W_e > 0$ and $W_s < 0$, we must have

$$\frac{dD}{ds} > 0, \quad \frac{dh}{ds} < 0, \quad \frac{d(h+D)}{ds} < 0.$$

Since the characteristics flow from the western and eastern boundaries toward the northern boundary at a central longitude, D must tend toward a maximum there, whereas both h and $h + D$ tend toward a minimum. Because of the different u_c in the two regimes, there will also be a different $\partial D/\partial x$ leading toward a southward component of deeper layer flow in the eastern regime and a northward one in the western regime. The quantitative details must be computed by numerical integration, as shown in the Figs. 6d, e and f.

The contours of h in Fig. 6d indicate a southward displacement in the western regime but, when the boundary B is crossed, they move northward (from the west). The depth D of the lower interface has contours that cross only the northern boundary (they cannot cross the western boundary by our choice of $D = D_0$). They define a great anticyclonic recirculation whose meridional direction changes sign at the regime boundary B.

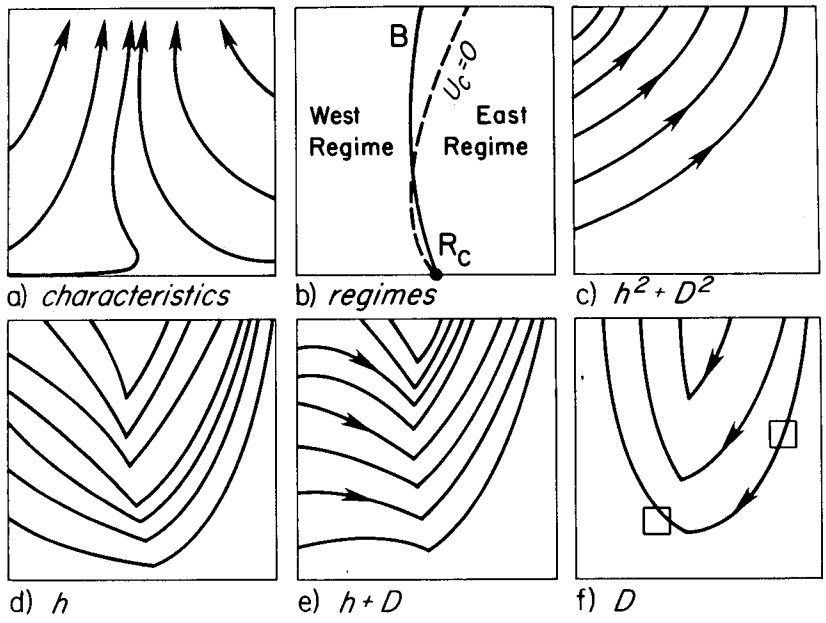

FIG. 6. Case B (southern half of a subpolar gyre): parameters $w_e = 3$ cm day^{-1}; $w_s = -3$ cm day^{-1}; $x_w = -2000$ km; midlatitude = 50°N; $h_0 = 150$ m; $D_0 = 200$ m; $g' = 0.01$ m s^{-2}. The panels show (a) paths of characteristics, (b) regimes and curve of $u_c = 0$, (c) Sverdrup transport function $h^2 + D^2$ (m^2) with contours of 5 m^2 and (d), (e), (f) the quantities h, $h + D$ and D with contours of 5,5 and 1 m, respectively.

The fluid velocity of the upper layer is determined by the geostrophic contours of $h + D$ as shown in Fig. 6e. They are not parallel to those of either h or D. The nonlinear Jacobian terms in the layer equations do not balance in the western regime. The upper layer water flows toward shallower h contours and hence passes through the upper interface with a horizontal component. In the eastern characteristic regime, however, the two nonlinear terms of the Jacobian do cancel each other and the interfacial flux is purely vertical. Here the old "law of parallel solenoids" does hold. This is in contrast to the state of affairs in the western regime that is dominated by a "cooling spiral." Furthermore, in the language of Luyten and Stommel (1985b) the direction of meridional flow in the eastern regime is such that the warm upper-layer water flows northwards and the lower-layer water flows southwards—it is in a sense a "direct" convective cell. In the western regime the situation is just the reverse—an "indirect" convective cell. It is also a region where, in contrast to Sverdrup balance alone, information can flow eastward from the western boundary current.

The effects of combining wind and buoyancy driving in the eastern regime may also be thought of as "additive" in the sense that being linear we can compute the Sverdrup transport in the gyre separately for both the wind and the buoyancy flux driving alone, and find the Sverdrup transports in each layer under the combination of the two agents by simple addition. This is not the case in the western regime, where the partition of Sverdrup meridional flows between the layers is more complicated through the nonvanishing Jacobian. Just how complicated is shown in Fig. 7 where the meridional components of upper and lower layer Sverdrup transport as functions of longitude along the midlatitude are displayed. The eastern regime is purely additive, whereas the partition between layers is much more complex in the western regime. The figures are obtained by placing a test point in the field of computation that records the local values of h and D and their slopes and does the calculation of the terms in the equations.

If the amplitudes of W_e and W_s are made larger, it is possible for the thickness h of the upper layer, or that, $D - h$ of the lower layer to vanish in some part of the field, thus forming a surface or subsurface "front". Figure 8 shows such a case where both events occur. When this happens the equations must be modified (the basic program easily accommodates this conditional logic) and the solutions continued.

If W_s vanishes in such regions beyond the fronts, as it might by definition, then the calculation proceeds by simple one-layer Sverdrup integration. The flow is out from under surface fronts in the subpolar gyre. Little new physics is involved at these fronts in the subpolar gyre, so we will not digress into a further discussion of them here.

5. Physics of the direct and indirect cells

In the discussion of the subpolar gyre's circulation we introduced the direct cell, for which, in a cooling

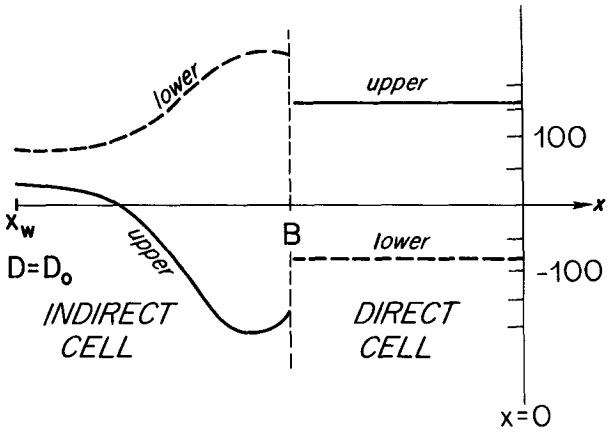

FIG. 7. Meridional transport in the upper (solid) and lower (dashed) layers across the midlatitude. The transition between the two regimes occurs where the section intersects the boundary, B. The actual solution is continuous across this boundary.

region the warm water flows northward toward the cooling whereas the lower layer flows southward. These occur in the eastern regime where the characteristics move westward from the eastern boundary. In the western regime, where the characteristics move eastwards from the western boundary the meridional flow is generally in the opposite sense: what we call the indirect cell.

There is a simple physical interpretation of these different meridional cells. For the subpolar gyre, case B (Fig. 6), in a cooling region, the interfacial flux w_s is from the warm layer to the cool layer, and by our definition negative. The vorticity equation

$$\beta v_1 = f\frac{\partial w_1}{\partial z}$$

gives us the true vertical component of velocity $w(-h)$ at the interface

$$w(-h) = w_e - \frac{\beta}{f} h v_1. \qquad (12)$$

If the cell is direct, ($v_1 > 0$) then the two velocities w_s

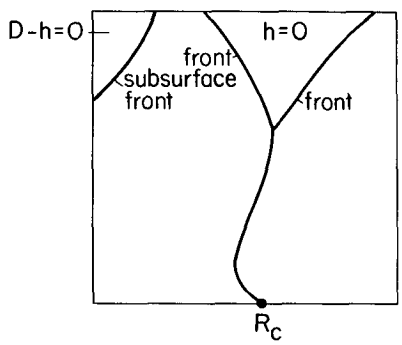

FIG. 8. Schematic illustration of the location of the fronts in a more strongly driven case (w_e = 6 cm day^{-1}, w_s = −8 cm day^{-1}).

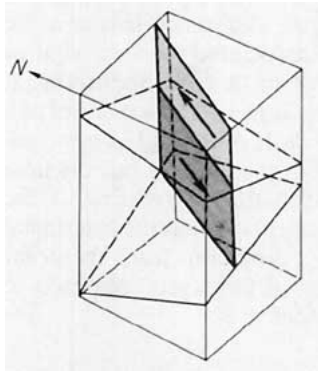

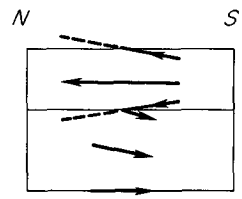

FIG. 9. Geometrical interpretation of the direct cell. The geometry of the layer interfaces is taken from the eastern regime in Case B (Fig. 6) as noted there in panel (a). The contours of $h + D$ and D are parallel as indicated. The true vertical velocity is the same sign as the interface flux.

and $w(-h)$ can have the same sign, provided v_1 is strong enough. Thus the water can flow directly downwards from the top to the lower layer as required. This behavior is seen in the region of the subpolar gyre, dominated by characteristics from the east, as illustrated in Fig. 9. The geometry of the layer interfaces is taken from Fig. 6. The planes with constant D and $h + D$ are parallel, and since w_s and $w(-h)$ are the same sign, the fluid can go directly from the top into the lower layer.

In the case of the indirect cell, we consider a region dominated by characteristics from the west. In the subpolar gyre, $v_1 < 0$ (see Fig. 6) so that the vertical component at the interface is upwards, whereas w_s is still negative. In this case, the geometry is more complicated, since the velocities v_1 and v_2 do not lie in the same plane. It is the strong zonal component of flows that permits the upper layer fluid to penetrate into the lower layer, despite the upward component of velocity in the indirect cell as illustrated in Fig. 10.

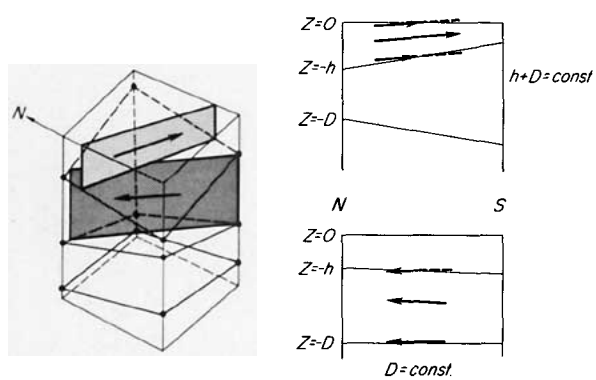

FIG. 10. Geometrical interpretation of the indirect cell. The geometry of the interfaces is taken from the western regime in Case B, (Fig. 6) as noted there in panel (a). The contours of D and $h + D$ are not parallel and are treated separately. In this case, the vertical velocity is upwards at the interface; it is the horizontal component of velocity which permits the fluid to pass from the upper layer into the lower layer.

We see, therefore, that the difference between the direct and indirect cells is associated with the sign of the vertical velocity relative to that of the interfacial flux w_s. In the direct cell the flow in the two layers can remain almost parallel to each other and is approximately two dimensional. For the indirect cell the flow is essentially three dimensional—the twisting of the flowlines with depth is the only way that the interfacial flux can be maintained in a direction (from the point of view of vertical ordering of the layers) opposed to that of the true vertical velocity.

Acknowledgments. We would like to acknowledge the generous financial support of the Office of Naval Research under Contract N00014-84-C-0134 NR 083-400 (JL) and of the National Science Foundation under Grant OCE83-14722 (HS). We are indebted to Dr. Nelson Hogg for a suggested improvement in the formulations of equations (5) and (6) at the eastern wall of the subtropical gyre.

REFERENCES

Luyten, J., and H. Stommel, 1985a: Upstream effects of the Gulf Stream on the structure of the mid-ocean thermocline. *Progress in Oceanography,* Vol. 14, Pergamon, 387–399.

——, and ——, 1985b. A Beta-control of buoyancy driven geostrophic flows. *Tellus,* (in press).

——, J. Pedlosky and H. Stommel, 1983: The ventilated thermocline. *J. Phys. Oceanogr.,* **13,** 292–309.

——, H. Stommel and C. Wunsch, 1985. A diagnostic study of the northern Atlantic Subpolar gyre. *J. Phys. Oceanogr.,* **15,** 1344–1348.

Rhines, P. B., and W. R. Young, 1982. A theory of the wind-driven circulation. I. Mid-ocean gyres. *J. Mar. Res.,* **40**(Suppl.), 559–596.

Stommel, H., 1957. The abyssal circulation. *Deep-Sea Res.,* **5,** 80–82.

Veronis, G., 1978. Model of world ocean circulation: III. Thermally and wind driven. *J. Mar. Res.,* **36,** 1–44.